BIOENG

Brazilian Journal of Biosystems Engineering (2025), 19 1298

REGULAR ARTICLE

PV energized EV motor using improved dolphin pod optimized PI controller with high gain Z source converter

B Kavya Santhoshi[1*]; Dondapati Ravi Kishore[1]; Anusuri Venkata Mani Govindu[2], Bhari Vinod Kumar[2], Kakana Boyina Rohit[2]

[1]Department of Electrical and Electronics Engineering, Godavari Global University, Rajahmundry, Andhra Pradesh, India
[2]Department of Electrical and Electronics Engineering, Godavari Institute of Engineering and Technology (A), Rajahmundry, India.

Regular Section
Academic Editor: Celso Antonio Goulart

Statements and Declarations

Data availability
All data will be shared on request.

Institutional Review Board Statement
Not applicable.

Conflicts of interest
The authors declare no conflict of interest.

Funding
This research did not receive any specific grant from funding agencies in the public, commercial, or non-profit sectors.

Autor contribution
BS: Conceptualization, Data Curation, Methodology, Writing-original draft, Writing-review and Editing; DK: Methodology, Project Administration, Supervision, Validation, Writing-review and Editing; AG: Methodology, Project Administration, Supervision, Validation, Writing-review and Editing; BK: Methodology, Project Administration, Supervision, Validation, Writing-review and Editing; KR: Methodology, Project Administration, Supervision, Validation, Writing-review and Editing.

Abstract

Photovoltaic (PV) based Electric Vehicle (EV) charging faces challenges of low voltage output, unstable supply, and limited converter performance under changing atmosphere condition. Hence, this work aims to develop a Permanent Magnet Synchronous Motor (PMSM) driven EV charging efficiency and stability using a novel converter and control approach. The major objective of this approach is to attain high efficient EV performance with improved stability and reliability. A High Gain Switched Quasi Z Source Converter (HG-SqZSC) is utilized for boosting the output voltage of PV with higher efficiency and increased voltage gain. An Improved Dolphin Pod (IDP)- optimised Proportional Integral (PI) controller is deployed to achieve a stable power output with increased convergence speed. On the other hand, during insufficient power supply or abnormal weather conditions, a three-phase grid and battery act as the supplementary power source, thereby providing continuous power supply required for PMSM motor-driven EV. Moreover, to validate the working and efficiency of the proposed PV-energized EV motor, MATLAB/Simulink is utilized which states that, the developed system ensures to attain higher efficiency (93.3%), Voltage gain (15) and reduced Total Hormonic Distortion (THD) (0.63%). Thus, it leads to less environmental pollution with constant EV charging systems even under varying circumstances.

Keywords

Photovoltaic (PV); High Gain Switched Quasi (HG-SqZSC); Improved Dolphin Pod (IDP); PI controller; Permanent Magnet Synchronous Motor.

This article is open access, under a Creative Commons Attribution 4.0 International License.

Introduction

EV's provides considerably efficient modes of transportation with reduced carbon emissions leading to environmentally safe driving (Saha et al., 2023; Sun et al., 2023). Although, EV's works utilizing motors as their driving mechanism, thus, they provide large starting torque and improved acceleration with reduced noise when compared to combustion engine-based vehicles. Prevailing motors like Brushless Direct current (BLDC) (Kumar et al., 2023; Kavin et al., 2024) and Switched Reluctance Motor (SRM) confers certain merits like enlarged life span and reduced power consumption with low maintenance cost, Nonetheless, these motor contain various demerits in comparable to merits, including larger noise, low torque, enlarged motor size, increased harmonics with excess heat generation (Shariff et al., 2019; Priyadarshi et al., 2022). Hence, to overcome these limitations, PMSM motor paves a vital part with its enhanced performance in terms of constant and high torque, minimized heat and smaller motor size (Huang et al., 2023). Despite these benefits, the integration of EVs with PV systems faces challenges because of the PV power output dependence on environmental conditions, such as irradiance and temperature, which cannot be relied upon as a sole energy source for charging EVs (Viswa Teja et al., 2023; Jayal & Bhuvaneswari, 2021). This condition requires efficient power conversion, and controller optimization and management of energy to maximize the continuous operation of the EV.

Charging PMSM driven EV's faces various difficulties (Anbuchandran, 2024), hence, to incorporate an effective EV charging process, PV system utilization is rising in recent days (Garcia-Trivino et al., 2023). There are various benefits associated with utilization of PV such as minimal cost implementation with easy and simple installation, furthermore, PV system requires minimal maintenance with very few components (González-Rivera et al., 2021).

Despite these benefits, PV is still not considered as a completely reliable source of energy supplier, this is due to the fact that their energy production depends on the environmental conditions (Katuri & Gorantla, 2023). Thus, to attain enhanced power output from PV, converters play a major part which boosts the PV power generation. Converters including Z-Source Converter (ZSC) (Liu et al., 2019), Z- Quasi Resonant (ZQR) (Poorali & Adib, 2019) and Switched Z-Source Quasi (Harini et al., 2022) are utilized for producing high voltage level outputs from PV, ZSC achieves highly efficient performance with higher power density, ZQR achieved increased boost function with varying load capacity and finally switched Z-Source converter obtained higher voltage gain

*Corresponding authors
E-mail address: kavyabe2010@gmail.com

https://doi.org/10.18011/bioeng.2025.v19.1298
Received:11 August 2025 / Accepted: 15 December 2025 / Available online: 19 April 2026

with better output power. However, even with all these benefits, these converters are still not applicable to produce the required power production for EV load. ZSC converters struggled with reduced boosting factor, minimizing power range with interrupted power supply. Nevertheless, conventional converters, struggle with voltage boost, limited power range and interrupted supplies. Considering these difficulties, a novel HG-SqZSC discussed in this proposed research archives higher gain, better efficiency and continuous power.

Moreover, it is vitally important to regulate and enhance the converter performance, thus PI controller is considered as an essential component. To achieve improved controller effectiveness, parameter tuning is requisite. Therefore, various optimization techniques are innovated for procuring enhanced parameter tuning such as Single Input Fuzzy Logic tuned deterministic Optimization (SIFL-DO), Grey Wolf Optimization (GWO) (Kanithi et al.), Genetic Algorithm Optimization (GAO) (Jiang & Zhen, 2019), Wild Horse Optimization (WHO) (Mazumdar et al., 2023). The implementation of these algorithms produced highly efficient tuning with increased response speed, accuracy, robustness, and fault tolerance with a better controller strategy (Rao et al., 2022).

Nevertheless, these algorithms remarkably go through several disadvantages which include time-consuming, require hyperparameter tuning which utterly increases the system complexity, requires additional iterations and very slow convergence rate. Henceforth, an IDP optimization algorithm is used, which achieves optimum tuning performance with faster response rate, enhanced accuracy and increased convergence rate. Additionally, battery and three phase grid system is deployed which gathers the excess energy produced by PV system and discharges it to EV load during an insufficient power supply from PV.

Thus, by utilizing the overall proposed techniques ensures to generate maximum power production that meet the EV load requirements with improved power quality, thereby providing sustainable and uninterrupted power supply. The fundamental contribution of the developed work is listed below.

- HG-SqZSC is integrated for generating higher-level output voltages to meet the power requirements of EV
- IDP optimized PI controller is implemented to assure optimum converter performance with regulated and stabilized output.
- PMSM motor is utilized for efficient functioning of EV
- Bi-directional converter is used on the battery side to ensure power supply back and forth.
- A Three phase Voltage Source Inverter (VSI) is deployed on the grid side for converting DC supply to AC, making is suitable for the grid.

Proposed modelling

For achieving continuous and stable EV charging, PV system plays a major part by providing clean and unlimited energy supply. Initially, PV produces low voltage output which does not meet the required voltage demand of PMSM driven EV load. Hence, it is essential to boost the PV power production, thus, this work utilizes a novel HG-SqZSC for acquiring increased voltage output supply needed for PMSM motor. The block diagram of the proposed system is illustrated in Figure 1.

Primarily, energy obtained from PV system is fed into the converter for obtaining higher voltage outputs, but voltage acquired by converter is not stable. Hence, to stabilize and to regulate converter output, IDP Optimized PI controller is attached, which produces balanced output thereby, improving the converter performance, to which the PWM generator is connected for providing PWM pulses. Later, output from converter flows via DC-bus to the three-phase VSI which converts DC to AC. Secondly, AC voltage produced by VSI is further fed to the PMSM motor that drives the EV load.

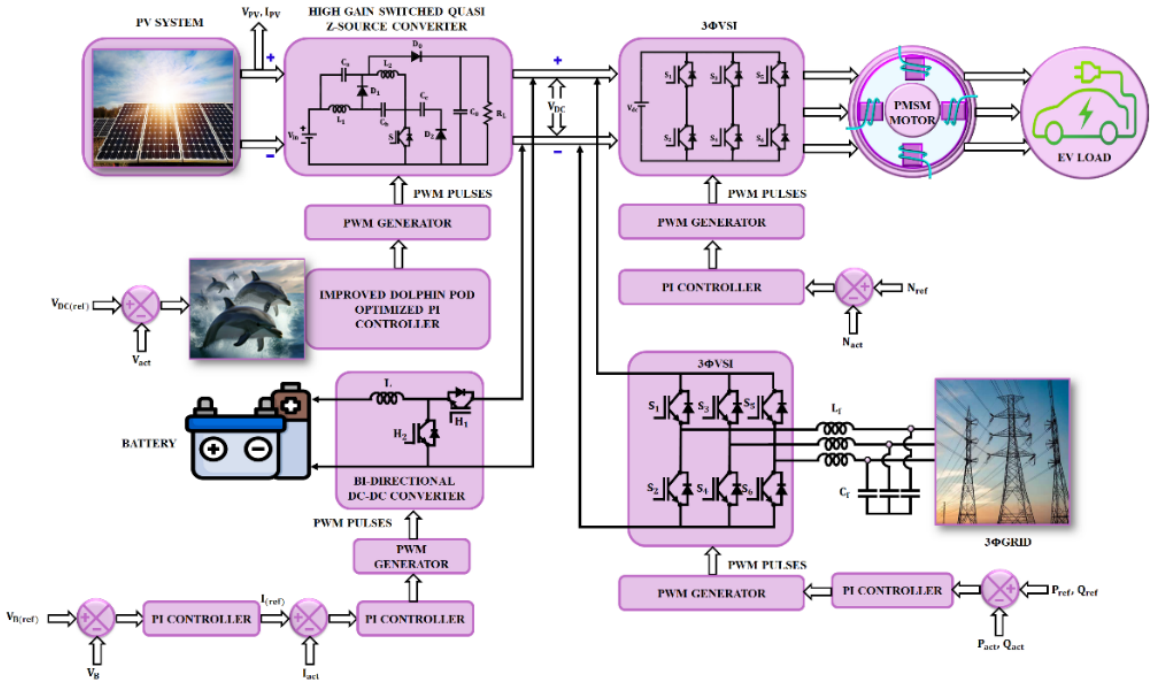

Figure 1. Block diagram of PV energized EV motor system.

Moreover, to assure better PMSM motor performance, PI controller is used for attaining improvised stability with reduced steady-state errors. In case of excess power production, the power supply is directed towards the three-phase grid through a three-phase VSI and to the battery through bidirectional converter, which eventually supplies power during higher load demand and acts as the supplementary power source during insufficient power issues, providing constant power supply to PMSM driven EV load. Therefore, the developed system ensures to provide constant and uninterrupted power supply to meet the desired voltage output level of PMSM motor.

Modelling of PV System

In this paper, PV system is utilized for providing unlimited power supply to the PMSM driven EV load. PV system generally constitutes one or more solar panels that absorb light energy and further convert it into electrical energy. PV system is given in Figure 2. where I_{ph} denotes the output current produced by the PV and I_r denotes the current across the resistor respectively.

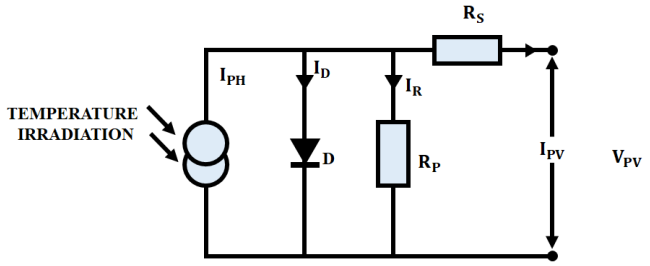

Figure 2. PV system Circuit Diagram.

Hence, the current across the resistor is given by,

$$I = I_{ph} - I_0 \quad (1)$$

However, the voltage generated by PV system is not completely reliable as they are influenced by the varying environmental conditions thereby providing low output voltages. Hence, to attain required voltage level to meet PMSM motor load demand, HG-SqZSC is utilized and is discussed in detail below.

Modelling of HG SqZSC

The HG-SqZSC consists of two inductors L_1 and L_2, capacitors C_a, C_b, C_c and C_0 and three diodes D_0, D_1 and D_2 are shown in Figure 3. respectively. The combination of switched capacitors with Quasi Z source enables to produce higher output voltage gain and its operating mode is classified into two as shown in Figure 4.

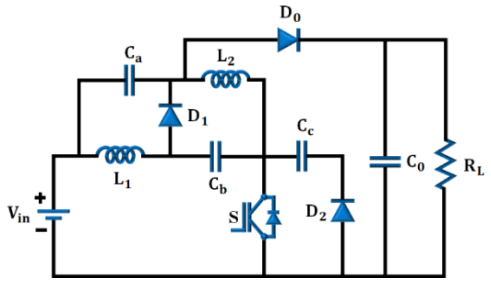

Figure 3. Proposed circuit of HG-SqZSC.

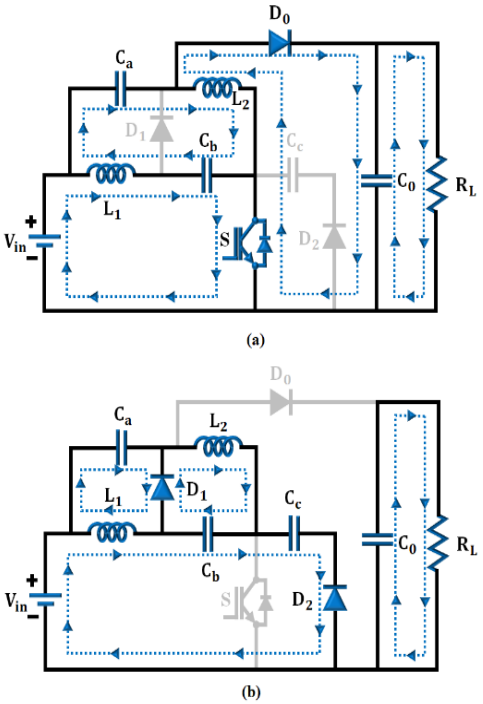

Figure 4. Converter modes of operation.

Mode 1: Here, Switch S is kept ON along with Diode D_0, whereas diodes D_1 and D_2 are turned OFF due to the reverse parallel connection. The inductor L_1 gets charged via input V_i and capacitor C_3 similarly, the inductor L_2 gets charged using V_i and C_1 respectively. Thus, making the capacitors C_1 and C_2 series to V_i.

According to Kirchoff voltage law,

$$V_{L1} = V_i + V_{C3} \quad (2)$$

$$V_{L2} = V_i + V_{C1} \quad (3)$$

$$V_0 = V_i + V_{C1} + V_{C2} \quad (4)$$

Mode 2: In this mode of operation, switch S is turned OFF along with diode D_0, whereas the diodes D_1 and D_2 are turned ON. Here, inductor L_1 gets charged through capacitor C_1 and L_2 gets charged via C_3, thus making V_i and L_1 series connection which is described as follows,

$$V_{L1} + V_{C1} = 0 \quad (5)$$

$$V_i = V_{L1} - V_{C3} + V_{C2} \quad (6)$$

$$V_i = V_{L1} - V_{C3} + V_{C2} \quad (7)$$

By considering the Volt-Second balance principle of the inductor,

$$V_{C1} = V_{C3} = \frac{D}{1-2D} V_i \quad (8)$$

$$V_{C2} = V_i + V_{C1} + V_{C3} = \frac{2-D}{1-2D} V_i \quad (9)$$

Where, Duty cycle of S is given as,

$$D = \frac{T_{on}}{T_s} \quad (10)$$

Where, T_{on} denotes the conduction time and T_s indicates the switching period.

Using eq (8) and (9) V_0 is derived as,

$$V_0 = V_i + V_{C1} + V_{C2} = \frac{2-D}{1-2D} V_i \quad (11)$$

Consecutively, the output voltage gain is evaluated using,

$$G = \frac{V_0}{V_1} = \frac{2-D}{1-2D} \quad (12)$$

When in continuous operation, the converter components of the HG-SqZSC such as inductors, capacitors, and devices experience a moderate level of thermal stress due to power conversion and switching losses. The high-efficiency design used, showcased by low THD (0.63%) and high voltage gain (15), helps to keep the heat generated due to losses to a manageable limit, which in return keeps the operational temperature within reasonable limits. Since the thermal management is capable, the degradation of the passive and active components will be minimized, thus extending the operational life of the components predominately to about 10–15 years at rated conditions, making the system reliable for continuous EV charging applications. Moreover, to improve the converter performance, controllers play an essential role, hence, an IDP optimized PI controller is utilized for attaining regulated and stabilized output power.

Modelling of Improved Dolphin Pod Optimized PI Controller

The IDP optimization algorithm is developed based on dolphin's hunting process. This hunting process of dolphin is exhibited in four stages.

Searching Stage

Call Stage

Reception Stage

Predation Stage

(i) Initialization: During the initial stage, each dolphin indicates a feasible solution and each dolphin is represented as $Dol_i = [x_1, x_2, \dots\dots, x_D]^T \quad (i = 1,2, \dots\dots, N)$, where N indicates the amount of dolphin and x_j $(j = 1,2, \dots\dots, D)$ represent the component of each dimension to be optimized. The two variables associated with the dolphin are Individual Optimum Solution denoted as L and the neighbourhood Optimum Solution which is denoted as K.

(ii) Pivotal Stages:

Search Stage: In this stage, Dolphin utilizes sound wave for searching its prey and is represented as,

$$V_i = [V_1, V_2, \dots\dots, V_D]^T \ (i = 1,2, \dots\dots, M) \quad (13)$$

where, M indicates the number of sound waves produced and $V_j = (j = 1,2, \dots\dots, D)$ denotes the dimension of each component. The sound waves produced by dolphin during the maximum search time T_1 enables to search for the optimum solution X_ijt which is expressed as,

$$X_{ijt} = Dol_i + V_j\, t \quad (14)$$

Call Stage: At this stage, the dolphin emits its sound waves along with its search results, to inform other neighbouring dolphins.

Reception Stage: In this stage, the results sent by the dolphin are compared with neighboring dolphin's optimum solution to determine the finest possible solution which is denoted as K_i.

Prediction Stage: The dolphins evaluate the radius R to predict the distance between the optimum solution of the neighboring dolphin and their location after the prediction stage based on the known information. Thus, producing the new position.

In addition to this, the output is then fed to the PMSM motor via the three phase VSI, which allows smooth conversion of DC to AC making it suitable for PMSM motor.

Modelling of PMSM Motor

PMSM is a permanent that contains a rotor and a stator parts as illustrated in Figure 5. in which the stator is made up of copper windings that are powered using a three-phase AC. The magnetic properties of PMSM enables them to obtain higher performance with great efficiency due to its high-power density, low mass and lower inertia. Additionally, permanent magnets are embedded to the rotor with field winding similar to that of the synchronous motor.

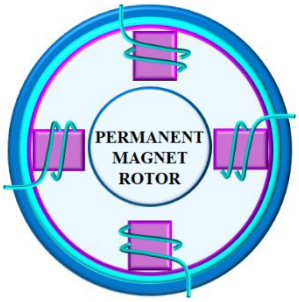

Figure 5. PMSM stator and Rotor.

The mathematical equation of PMSM is given by,

$$\frac{d\omega}{dt} = \frac{3P\,\lambda_m}{2j}\, i_q - \frac{B}{j}\,\omega - \frac{T_L}{j} \quad (15)$$

$$\frac{di_q}{dt} = \frac{R}{L}\, i_q - P\omega i_d - \frac{P\lambda_m}{L}\,\omega + \frac{1}{L}\, V_q \quad (16)$$

$$\frac{di_d}{dt} = -\frac{R}{L}\, i_d + P\omega i_q + \frac{1}{L}\, V_d \quad (17)$$

Where, ω represents the angular speed of the rotor, P represents the number of pole pairs, λ_m denotes the rotor magnetic flux, j is the rotor inertia, B denotes the friction factor, T_L indicates the load torque, i_q represents the q-axis current, i_d is the d-axis current, V_q is the q-axis voltage, V_d represents d-axis voltage, R is the stator resistance and L denotes the stator inductance respectively. The voltages across stator are given by,

$$\begin{pmatrix} V_a \\ V_b \\ V_c \end{pmatrix} = R_s \begin{pmatrix} I_a \\ I_b \\ I_c \end{pmatrix} + \frac{dL_{ss}}{dt} \begin{pmatrix} I_a \\ I_b \\ I_c \end{pmatrix} \psi_r \frac{d}{d\theta_e} \begin{pmatrix} \cos(\theta_e) \\ \cos(\theta_e - 2\pi/3) \\ \cos(\theta_e + 2\pi/3) \end{pmatrix} \quad (18)$$

Where, V_a , V_b and V_c represents the stator voltages, I_a , I_b and I_c denotes the stator currents, L_{ss} represents stator inductance, ψ_r indicates the flux linkages and θ_e represents the rotor angle respectively. Furthermore, with the aid of PI controller, grid synchronization is achieved, which is discussed below.

Grid Synchronization

The synchronous PI control approach is utilized in a two-phase rotating $(d-q)$ frame, this control approach attains sinusoidal control. According to the synchronous control approach, three-phase grid voltage and current attains DC variables, PI controller is adapted, so that current loop achieves no steady-state errors. The grid voltage is given as,

$$\begin{cases} u_{sa} = U_m \sin \omega t \\ u_{sb} = U_m \sin(\omega t - 2\pi/3) \\ u_{sc} = U_m \sin(\omega t + 2\pi/3) \end{cases} \quad (19)$$

This approach enables to attain the merits of synchronous rotating frames, thus, active and reactive current is decoupled and controlled respectively. Overall, the proposed system enables enhanced utilization of PV with improved PMSM motor performance, thus attaining effective EV charging.

Results and discussion

The developed system using HG-SqZSC and IDP optimized PI controller for PMSM motor utilized EV charging, is evaluated using MATLAB/Simulink and its obtained results are detailed and analyzed in this section along with their comparative analysis.

Constant Temperature and Constant Intensity

Figure 6 represents solar temperature and intensity waveform, where both temperature and intensity remain consistent and stable at $35° C$ *and* $1000\, W/sq-m$ respectively, throughout the depicted time period, ensuring improved PV system performance. This steady state assures that the PV array delivers expected and maximum power output which ultimately influences the charging efficiency to the EV system. Furthermore, the steady irradiance allows the DC link voltage to remain stable while reducing variations in the PMSM drive which impacts the interface with the grid while allowing for smooth operation of the EV system.

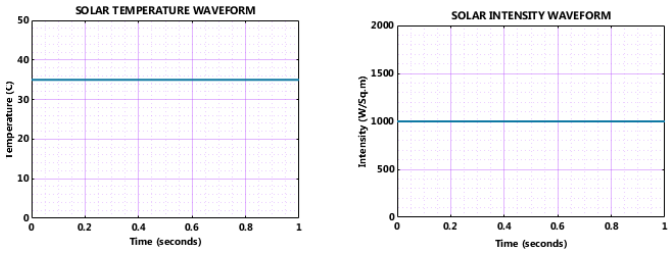

Figure 6. Temperature and intensity Waveform under constant conditions.

Figure 7 indicates input DC voltage and Input DC current, the first graph shows that input voltage is maintained at $100V$ for the entire depicted time and the second graph shows that input current is also maintained at $95A$ through the given time period, indicating improved system stability with increased power reliability. The stability of voltage and currents reflects an enhanced reliability of the system by providing consistent power to the EV based PMSM Drive while supporting stable operation of the grid-connected PV system.

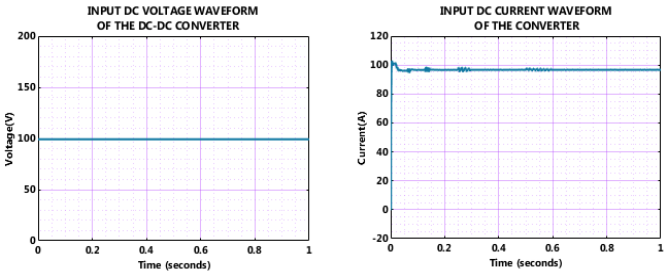

Figure 7. Input DC voltage and current Waveform under constant conditions.

Figure 8 implies DC-DC output voltage, which initially deviates, after 0.1 seconds stabilizes and remains fixed at $600\, V$. Similarly, output current also initially fluctuates and then stabilizes after 0.1 seconds respectively. This quick stabilization in the presence of consistent solar levels shows that the converter effectively regulates voltage and current to the EV based PMSM drive ensuring reliable power delivery and stability in the grid-controlled operation.

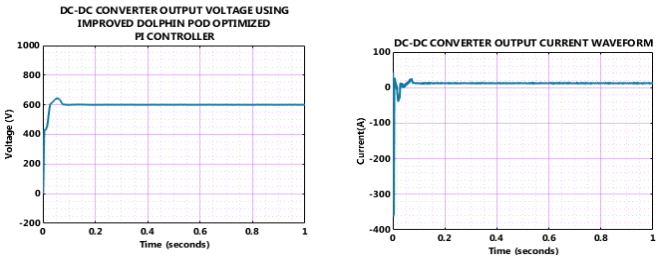

Figure 8. Output DC-DC converter voltage and current waveform under constant condition.

Figure 9 illustrates the input and output power waveforms for the system. The input power quickly rises to $10{,}000\, W$ and experiences some minor drop to $9{,}990\, W$ before stabilizing and the output power initially fluctuates slightly before stabilizing after about 0.1 s. This shows that the system reaches steady conditions after approximately 0.1 s which depicts efficient power transfer from the PV source to the EV based PMSM drive while allowing for consistent power delivery during grid-controlled operation.

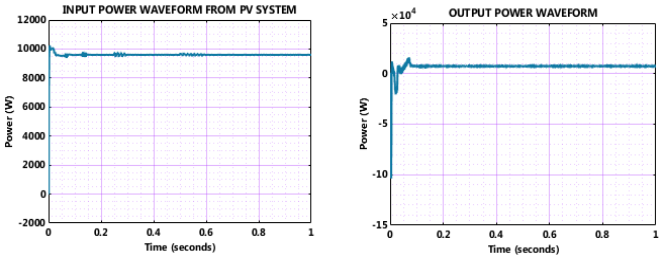

Figure 9. Input and output power under constant conditions.

In Figure 10, the characteristics of the battery SOC, voltage, and current are presented. The SOC is held at 60% for the entire time period; the voltage is held at $125\, V$ throughout the test, indicating stability. The voltage and current waveforms are smooth and consistent, suggesting stable operating conditions. This consistency demonstrates the efficiency of the battery management strategy, providing a dependable energy supply to the EV based PMSM system and a reliable interaction with the grid.

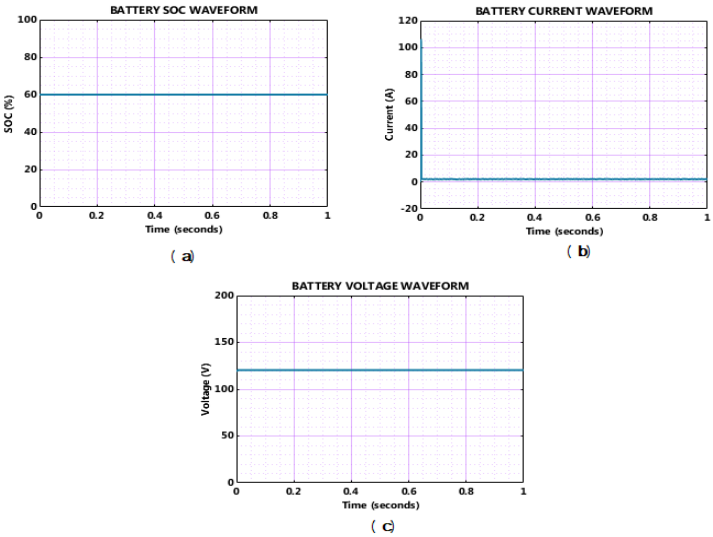

Figure 10. Characteristics waveform of battery under constant conditions.

Figure 11. showcases grid voltage and current in sinusoidal wave representations, where voltage ranges between $\pm 400\ V$ and current ranges between $\pm\ 12\ A$ respectively. The third graph shows the combination of both grid voltage and current waves, which showcases optimum grid by achieving perfect grid synchronization. This indicates that grid synchronization occurs to provide reliable operation of the grid and reliable power transfer between the PV based EV system and the utility grid.

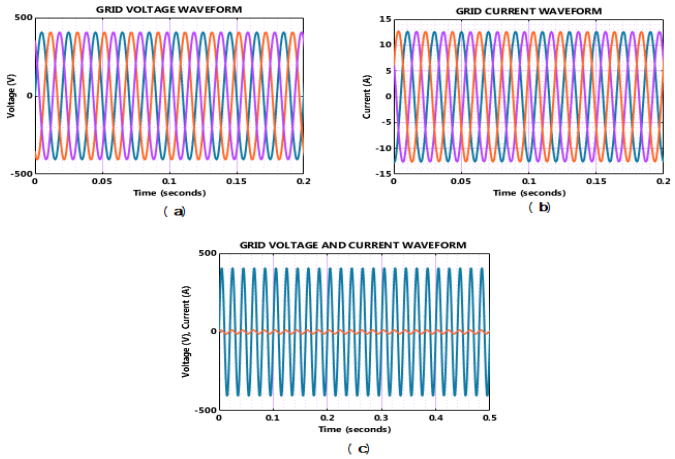

Figure 11. Grid voltage and current waveforms under constant conditions.

Figure 12 represents three phase inverter voltage waveforms with and without filter, the first graph shows the voltage attained without using filter, where voltage keeps fluctuating and contains unwanted interferences, while second graph comprises voltage waveform with filter shows stabilized voltage ranging between$\pm\ 400V$, providing improved power quality. This analysis illustrates the filters' effectiveness in decreasing harmonics and therefore enhancing quality of power in both grid and the PMSM drive.

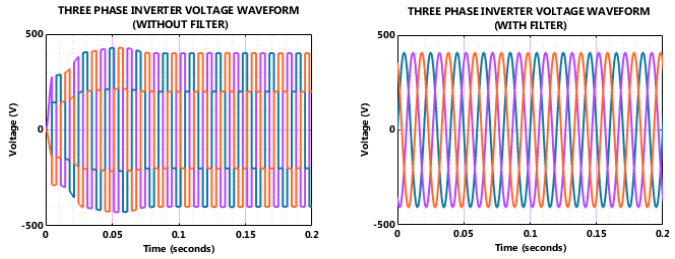

Figure 12. Three phase inverter voltage waveforms without and with filter under constant conditions.

Figure 13 indicates the real and reactive power waveform, in which both reactive and real power remain fixed. From the above graph it is understandable that real power attained is relatively higher than that of reactive power, indicating reduced power losses and effective working of the proposed system. This relationship demonstrates reductions in power losses and more effective use of supplied energy. The stability of the power profiles also illustrates the effectiveness of the proposed converter and control strategy to enable reliable operation of the PMSM drive and its functioning in relation to the grid.

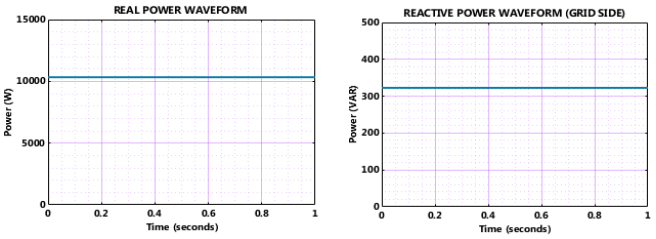

Figure 13. Real and Reactive power waveform under constant conditions.

Varying Temperature and Varying Intensity

Figure 14. denotes varying temperature and intensity of solar, where temperature at first is maintained at $25°\ C$ and at 0.4 seconds temperature slightly raises and stays fixed at $35°\ C$. Similarly, solar intensity is maintained at 800 W/Sq-m, after 0.6 seconds, solar intensity increases to $1000\ W/Sq-m$ to remain stable. These changes are dependent on the dynamic performance of the PV system, which emphasizes the importance of converter and controller design and capability to conduct stable EV charging through changing conditions.

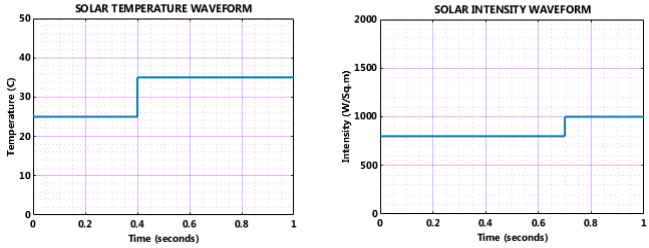

Figure 14. Solar temperature and intensity waveform under varying conditions.

Figure 15. implies input DC voltage and current waveform, where voltage progressively keeps increasing and stabilizes at $100\ V$ after 0.6 seconds, Meanwhile, current at first rapidly increases beyond $80\ A$ and then fluctuates, after 0.6 seconds current stabilizes at $90A$ respectively. This action emphasizes that the system is successfully able to handle transient variations and achieve steady operation to reliably deliver power to the PMSM drive.

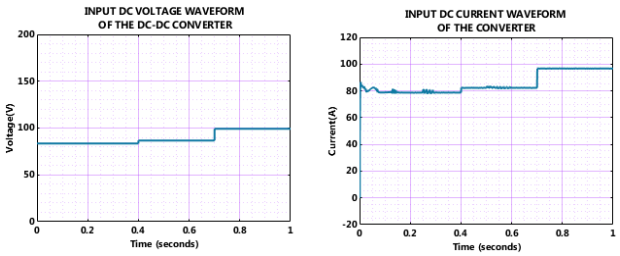

Figure 15. Input DC voltage and current waveform under varying conditions.

Figure 16. implies DC-DC converter output voltage and current waveform, the first graph shows that output voltage deviates in the beginning and further stays constant at $600\ V$ throughout the depicted time duration. Current waveform demonstrates that current with initial fluctuations and later remains constant respectively. These results support that the converter is able to control the output effectively in a steady manner to allow reliable power delivery to the PMSM drive from the original variations in input.

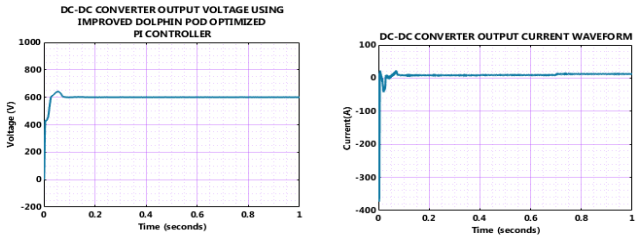

Figure 16. Output voltage and current of DC-DC converter under varying conditions.

Figure 17. refers to the input and output power waveform for PV system in which, the input power shows certain deviation with gradual increase and after 0.6 seconds, the input power rises to 9990 W respectively. The graph showcasing output power depicts output power remains fixed, ensuring effective performance.

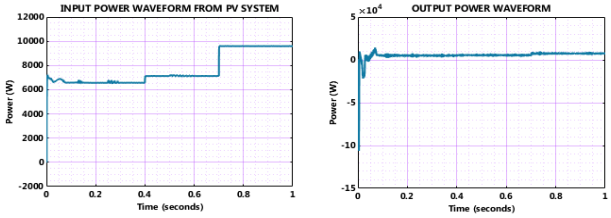

Figure 17. Input and output from PV system under varying conditions.

Figure 18 shows the SOC, current, and voltage of the battery under varying operational conditions. The SOC is constant at 60% over the entire period demonstrating effective energy management. The battery current and battery voltage waveforms both show stable, consistent waveforms demonstrating that the control strategy is robust. The stability of the battery power system indicates it is reliable under the varying outside environmental variations, supplies or absorbs power as needed for the PMSM drive and serves as a consistent energy storage to stabilize power delivery from the solar panels.

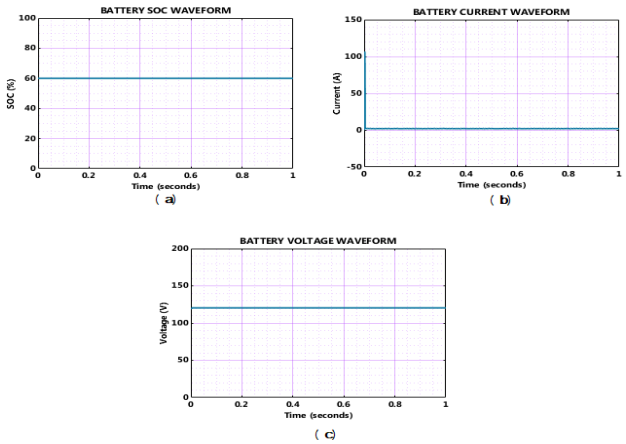

Figure 18. Battery SOC, current and voltage under varying conditions.

Figure 19. represents the voltage and current waveform of the grid, where both voltage and current depict consistent and stable voltage ranging between $\pm$ 400 V and current ranging between $\pm 12\,A$ respectively. The third graph showcases voltage together with current, and their perfect synchronization indicates improved grid functioning efficacy. Establishing synchronization establishes a reliable power interface between the PV–EV system and the utility grid, thus confirming the validity of the robustness of the control strategy.

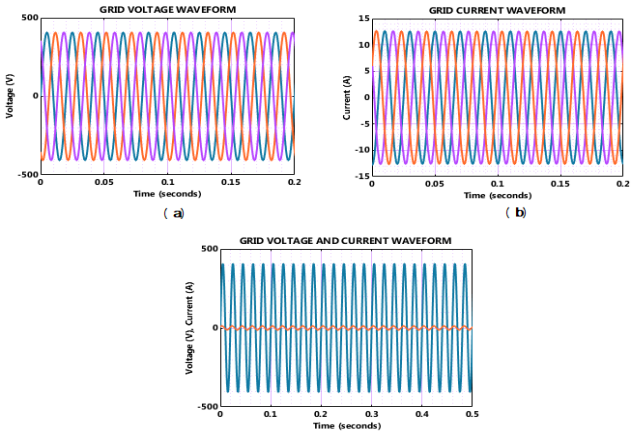

Figure 19. Voltage and current waveform for grid under varying conditions.

Figure 20. Figure 20 showcases voltage waveform for three phase inverter with and without filter, where the voltage waveform without a filter shows certain fluctuations with unwanted disturbance. While voltage waveform with filter shows consistent and stable waves ranging between $\pm$ 400 V respectively. This shows the importance of the filtering stage regarding harmonics reduction, distortion mitigation, and power quality enhancement for the grid and, indeed, the PMSM drive.

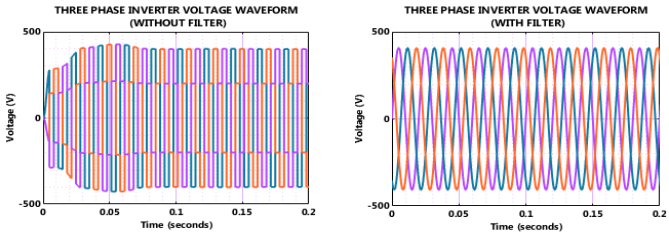

Figure 20. Voltage waveform for three phase inverter without and with filter under varying conditions.

Figure 21 presents real and reactive power signatures of the system when it experiences diverging operating conditions. Real power remains relatively constant at around 10,100 W while the reactive power is also held constant at nearly 310 W through the 1s duration. The much lower value of reactive versus real power demonstrates that power is being used efficiently and not being wasted. These steady metrics demonstrate that the proposed converter and control strategy achieve energy transfer and reliable operation of the overall system.

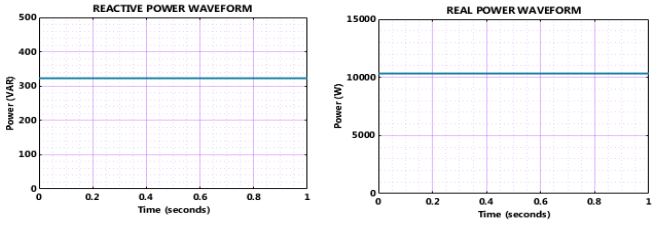

Figure 21. Reactive and real power under varying conditions.

Figure 22. demonstrates PMSM motor speed, torque and current waveform, in the first graph the PMSM motor speed progressively increases to 1000 RPM at 0.2 seconds, then motor speed is maintained at that speed. From the second graph it is notable that, PMSM torque considerably low at $1\ N-m$. And third graph showcases that, PMSM motor current initially fluctuates anf further is maintained at constant respectively.

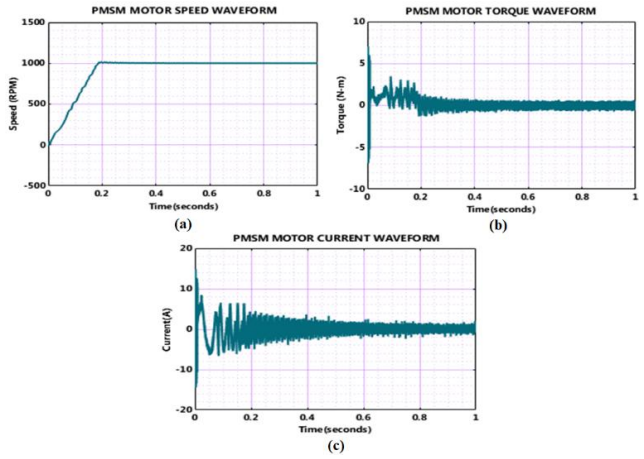

Figure 22. PMSM speed, torque and current waveform.

Figure 23. represents PMSM motor stator current for three phases namely, (a) Phase A , (b) Phase B and (c) Phase C, where all the three phases shows initial oscillations and further stabilizes. Of the three phases, Phase A and Pahse B depicts slightly higher initial oscillation when compared to Phase C, All the three graph depicts the motor's characteristics of increased stability.

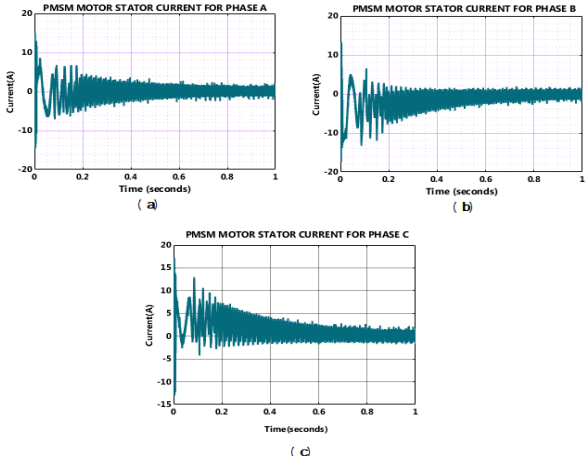

Figure 23. PMSM motor stator current.

Figure 24. shows the THD waveforms, where in Figure 24 (a) depicts highest THD is 1%, referring to certain harmonic distortion, while Figure 24 (b) exhibits slightly reduced THD of 0.88% than that of the first graph, indicating lightly minimized harmonics and interferences. Whereas Figure 24 (c) reduced THD of 0.68% when compared all three graphs, ensuring minimized harmonics with highest magnitude at the fundamental frequency respectively.

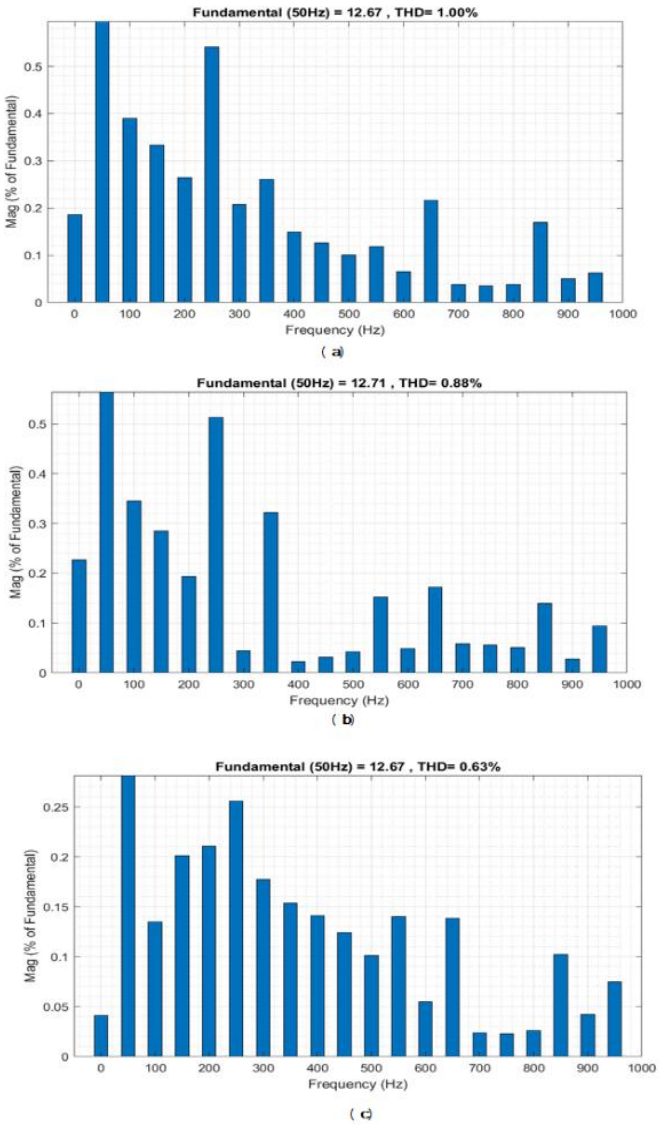

Figure 24. Three phase THD waveform.

Figure 25. represents graph comprising of Voltage gain comparison between proposed converter and various conventional converters. From the above graph it is depictable that the proposed converter attained higher voltage of (15), than that of the conventional converter such as Hybrid ZSC (10), Step-up Quasi ZSC (6) and Soft switch ZSC (4) respectively.

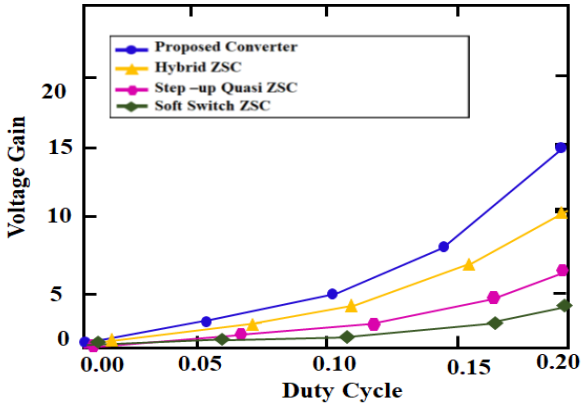

Figure 25. Voltage Gain Comparison

Figure 26. depicts the Efficiency comparison chart, where conventional converters like SC-DC DC (Stala et al., 2020), HS-SZC (Kumar et al., 2021) and ZVS converter (Folmer & Stala, 2021) are analyzed in terms of efficiency, to evaluate the efficiency of the proposed converter. This chart shows that conventional converter shows slightly reduced efficiency of (91%), (92.50%) and (92.8%) than that of the proposed converter which acquired (93.3%) respectively, indicating enhanced converter performance.

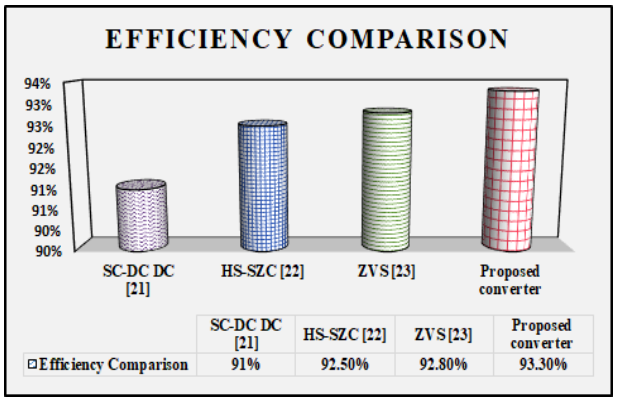

Figure 26. Efficiency Comparison

Figure 27. shows MSE comparison for Improved Dolphin Optimized PI controller, with conventional PI controller optimized using Differential Evaluation (DE) Algorithm. The above chart represents the MSE comparison for three iterations, in which proposed algorithm obtained reduced MSE in all the three iterations when compared to DE optimized PI controller. Thus, achieving improved control performance.

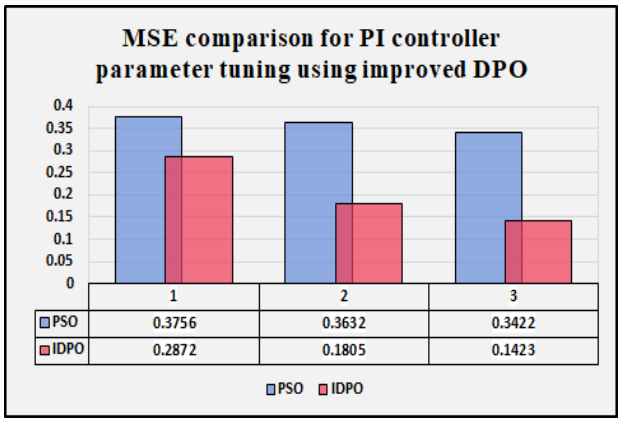

Figure 27. MSE Comparison

Figure 28. indicates THD comparison chart, from which it is, evident that, the proposed converter achieves reduced THD of (0.68%), ensuring highly minimized harmonics. Whereas conventional converters showcase slightly higher THD of (1.60%), (1.34%) and (0.93%), which indicates higher harmonics rate when compared to proposed converter.

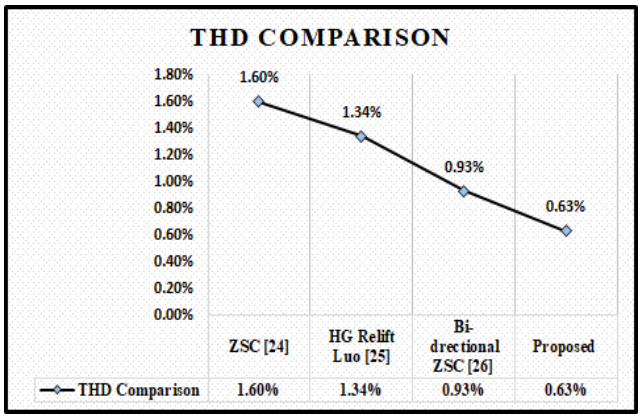

Figure 28.THD Comparison

Conclusions

This paper proposes the integration of HG-SqZSC with IDP optimized PI controller for producing enhanced output voltage to power the PMSM driven EV load. The deployment of HG-SqZSC ensures attaining higher output voltages to run the PMSM motor with enhanced efficiency, and Voltage gain. In addition to that, the implementation of IDP optimized PI controllers to improve the converter performance, thereby providing stable output with increased convergence speed and reduced fluctuations and oscillations thereby, achieving proficient system functioning. In contrast, during limited power production, battery and gird acts as the supplementary power supply, henceforth, providing consistent and sustainable power supply even under varying circumstances.

The suggested system is unlimitedly scalable, as the HG-SqZSC topology and control scheme is scaled to higher power levels by advancing the device ratings as well as using a modular system. Therefore, efficiency and reliability are achieved when implementing the solution for larger vehicles as well as public charging stations.

Further, MATLAB/Simulink results demonstrate that proposed work attained higher efficiency (93.3%) with enhanced voltage gain (15) and reduced THD (0.63%) with increased convergence speed.

Therefore, this work provides positive impacts on environmentally safe transportation with minimized expenses thus leading to limited emission of harmful gases. Future efforts will include empirical validation of the proposed system, analysis of implementation complexity and cost-effectiveness, and environmental benefit quantification in real world EV charging practices.

References

Aandal, R., & Ravi, A. (2024). Design of Z source converter with the genetic-based chicken swarm algorithm for closed loop control of PV integrated grid. *Automatika, 65*(3), 675–690. https://doi.org/10.1080/00051144.2024.2308463

Agrawal, Y. K., & Tandon, S. G. (1971). N-arylhydroxamic acids. *Journal of Chemical & Engineering Data, 16*(4), 495–496. https://doi.org/10.1021/je60051a004

Anbuchandran, S., Babu, M. A., Stephen, D. S., & Thinakaran, M. (2024). DC microgrid for EV charging station with EV control by using STSM controllers. *Engineering Research Express, 6*(4), 045345. https://doi.org/10.1088/2631-8695/ad92d9

Folmer, S., & Stala, R. (2021). DC-DC high voltage gain switched capacitor converter with multilevel output voltage and zero-voltage switching. *IEEE Access, 9*, 129692–129705. https://doi.org/10.1109/ACCESS.2021.3111546

Garcia-Trivino, P., de Oliveira-Assis, L., Soares-Ramos, E. P., Sarrias-Mena, R., Garcia-Vazquez, C. A., & Fernandez-Ramirez, L. M. (2023). Supervisory control system for a grid-connected MVDC microgrid based on Z-source converters with PV, battery storage, green hydrogen system and charging station of electric vehicles. *IEEE Transactions on Industry Applications, 59*(2), 2650–2660. https://doi.org/10.1109/TIA.2022.3233556

González-Rivera, E., García-Triviño, P., Sarrias-Mena, R., Torreglosa, J. P., Jurado, F., & Fernández-Ramírez, L. M. (2021). Model predictive control-based optimized operation of a hybrid charging station for electric vehicles. *IEEE Access, 9*, 115766–115776. https://doi.org/10.1109/ACCESS.2021.3106145

Harini, S., Chellammal, N., Chokkalingam, B., & Mihet-Popa, L. (2022). A novel high gain dual input single output Z-quasi resonant (ZQR) DC/DC converter for off-board EV charging. *IEEE Access, 10*, 83350–83367. https://doi.org/10.1109/ACCESS.2022.3195936

Huang, Q., Huang, Q., Guo, H., & Cao, J. (2023). Design and research of permanent magnet synchronous motor controller for electric vehicle. *Energy Science & Engineering, 11*(1), 112–126. https://doi.org/10.1002/ese3.1316

Jayal, P., & Bhuvaneswari, G. (2021). A novel space vector modulation-based transistor-clamped H bridge inverter-fed permanent magnet synchronous motor drive for electric vehicle applications. *International Transactions on Electrical Energy Systems, 31*(3), e12789. https://doi.org/10.1002/2050-7038.12789

Jiang, W., & Zhen, Y. (2019). A real-time EV charging scheduling for parking lots with PV system and energy store system. *IEEE Access, 7*, 86184–86193. https://doi.org/10.1109/ACCESS.2019.2925559

Kanithi, H., Pappu, P.P., & Das, P.K. Emotions in storybooks: Simulation and Analysis of Switched-Z-Source/Quasi-Z-Source DC-DC Converters. https://doi.org/10.9790/9622-1101055055

Katuri, R., & Gorantla, S. (2023). Design and comparative analysis of controllers implemented to hybrid energy storage system based solar-powered electric vehicle. *IETE Journal of Research, 69*(7), 4566–4588. https://doi.org/10.1080/03772063.2021.1941328

Kavin, K. S., Subha Karuvelam, P., Devesh Raj, M., & Sivasubramanian, M. (2024). A novel KSK converter with machine learning MPPT for PV applications. *Electric Power Components and Systems*, 1–19. https://doi.org/10.1080/15325008.2024.2346806

Kumar, N., Singh, H. K., & Niwareeba, R. (2023). Adaptive control technique for portable solar powered EV charging adapter to operate in remote location. *IEEE Open Journal of Circuits and Systems, 4*, 115–125. https://doi.org/10.1109/OJCAS.2023.3247573

Kumar, R., Kannan, R., Nor, N. B. M., & Mahmud, A. (2021). A high step-up switched Z-source converter (HS-SZC) with minimal components count for enhancing voltage gain. *Electronics, 10*(8), 924. https://doi.org/10.3390/electronics10080924

Liu, J., Wu, J., Qiu, J., & Zeng, J. (2019). Switched Z-source/quasi-Z-source DC-DC converters with reduced passive components for photovoltaic systems. *IEEE Access, 7*, 40893–40903. https://doi.org/10.1109/ACCESS.2019.2907300

Mazumdar, D., Biswas, P. K., Sain, C., & Ustun, T. S. (2023). GAO optimized sliding mode based reconfigurable step size Pb&O MPPT controller with grid integrated EV charging station. *IEEE Access, 12*, 10608–10620. https://doi.org/10.1109/ACCESS.2023.3344275

Poorali, B., & Adib, E. (2019). Soft-switched high step-up quasi-Z-source DC–DC converter. *IEEE Transactions on Industrial Electronics, 67*(6), 4547–4555. https://doi.org/10.1109/TIE.2019.2922948

Prakash, S., Boopathy, K. (2024). Hybrid MGWO-CSO optimized high gain Relift Luo converter for PV based grid tied PMBLDC drive system. *Measurement: Sensors*, *31*, 101010. https://doi.org/10.1016/j.measen.2023.101010

Priyadarshi, N., Bhaskar, M. S., Azam, F., Singh, M., Dhaked, D. K., Taha, I. B., & Hussien, M. G. (2022). Performance evaluation of solar-PV-based non-isolated switched-inductor and switched-capacitor high-step-up Cuk converter. *Electronics, 11*(9), 1381. https://doi.org/10.3390/electronics11091381

Rao, C. S. P., Pandian, A., Reddy, C. R., Aymen, F., Alqarni, M., & Alharthi, M. M. (2022). Location determination of electric vehicles parking lot with distribution system by Mexican axolotl optimization and wild horse optimizer. *IEEE Access, 10*, 55408–55427. https://doi.org/10.1109/ACCESS.2022.3176370

Saha, B., Singh, B., & Sen, A. (2023). SMO-based position sensorless BLDC motor drive employing canonical switching cell converter for light electric vehicle. *IEEE Transactions on Industry Applications, 59*(3), 2974–2984. https://doi.org/10.1109/TIA.2023.3241607

Shariff, S. M., Alam, M. S., Ahmad, F., Rafat, Y., Asghar, M. S. J., & Khan, S. (2019). System design and realization of a solar-powered electric vehicle charging station. *IEEE Systems Journal, 14*(2), 2748–2758. https://doi.org/10.1109/JSYST.2019.2931880

Shyamprasad, M., & Saravanan, M. (2023). Emotions in storybooks: Three-Phase of Bi-Directional Z-Source Converters for Vehicle-To-Grid Applications a Low-Harmonic and Fuzzy Logic Control Method. *IRJET,* 10.

Stala, R., Waradzyn, Z., & Folmer, S. (2020). DC-DC high-voltage-gain converters with low count of switches and common ground. *Energies, 13*(21), 5657. https://doi.org/10.3390/en13215657

Sun, Q., Xie, H., Liu, X., Niu, F., & Gan, C. (2023). Multiport PV-assisted electric-drive-reconstructed bidirectional charger with G2V and V2G/V2L functions for SRM drive-based EV application. *IEEE Journal of Emerging and Selected Topics in Power Electronics, 11*(3), 3398–3408. https://doi.org/10.1109/JESTPE.2023.3240434

Viswa Teja, A., Razia Sultana, W., & Salkuti, S. R. (2023). Performance explorations of a PMS motor drive using an ANN-based MPPT controller for solar-battery powered electric vehicles. *Designs, 7*(3), 79. https://doi.org/10.3390/designs7030079